doi.org/10.15392/2319-0612.2025.2841
Braz. J. Radiat. Scci., Rio de Janeiro
2025, 13(2) | 01-21 | e2841
Submitted: 2025-01-27
Accepted: 2025-04-10

Photon shielding properties of TiO_2 and WO_2 incorporated into ordinary concrete: Evaluation for radiotherapy applications

Moreto [a], C. B.; De Paiva [a*], E.

[a] Institute of Radiation Protection and Dosimetry, 22783-127, Rio de Janeiro, RJ, Brazil.

*Correspondence: eduardo.paiva@ird.gov.br

Abstract: This computational study evaluates the photon shielding properties of titanium dioxide (TiO_2) and tungsten dioxide (WO_2) when incorporated into ordinary concrete. The analysis utilizes the National Institute of Standards and Technology (NIST) XCOM database to calculate mass attenuation coefficients, tenth-value layers (TVL), mean-free paths (MFP), and radiation protection efficiency (RPE) over photon energies ranging from 1 to 10 MeV. Results demonstrate that concrete enhanced with TiO_2 and WO_2 shows a significant improvement in photon shielding efficiency compared to conventional concrete, particularly at higher photon energy. At 6 MeV, TVL for ordinary concrete is 46% higher than TVL for the sample in which 50% of the gravel was replaced by TiO_2 (by volume), and is 237% higher than the TVL for the sample when considering the incorporation of WO_2 in the same proportion. At 10 MeV, these differences change to 42% and 338%, respectively for the samples containing TiO_2 and WO_2. These findings highlight the superior shielding properties of the TiO_2 and WO_2 composites, suggesting that they have strong potential for applications in radiotherapy facility rooms and nuclear systems shielding. Experimental validation of these computational results is planned for future work to further confirm their practical applicability.

Keywords: photon attenuation, shielding materials, TiO_2, WO_2.

doi.org/10.15392/2319-0612.2025.2841
Braz. J. Radiat. Scci., Rio de Janeiro
2025, 13(2) | 01-21 | e2841
Submitted: 2025-01-27
Accepted: 2025-04-10

Propriedades de blindagem de fótons do TiO_2 e WO_2 incorporados em concreto comum: Avaliação para aplicações em radioterapia

Resumo: Este estudo computacional avalia as propriedades de blindagem de fótons do dióxido de titânio (TiO_2) e do dióxido de tungstênio (WO_2) quando incorporados ao concreto comum. A análise utiliza o banco de dados XCOM do National Institute of Standards and Technology (NIST) para calcular os coeficientes de atenuação de massa, as camadas deci-redutoras (TVL), os livres caminhos médios (MFP) e a eficiência de proteção contra radiação (RPE) em energias de fótons que variam de 1 a 10 MeV. Os resultados demonstram que o concreto acrescido de TiO_2 e WO_2 apresenta uma melhoria significativa na eficiência de blindagem de fótons em comparação com o concreto convencional, particularmente em energias de fótons mais altas. Em 6 MeV, o TVL para concreto comum é 46% maior que o TVL para a amostra na qual 50% da brita foi substituída por TiO_2 (por volume), e é 237% maior que o TVL para a amostra quando se considera a incorporação de WO_2 na mesma proporção. Em 10 MeV, essas diferenças mudam para 42% e 338%, respectivamente, para as amostras contendo TiO_2 e WO_2. Essas descobertas destacam as propriedades de blindagem superiores dos compostos de TiO_2 e WO_2, sugerindo que eles têm forte potencial para aplicações em salas de instalações de radioterapia e blindagem de sistemas nucleares. A validação experimental desses resultados computacionais está planejada para trabalhos futuros, de modo a confirmar sua aplicabilidade prática.

Palavras-chave: atenuação de fótons, materiais de blindagem, TiO_2, WO_2.

1. INTRODUCTION

Radiotherapy is a cornerstone in the treatment of various malignancies, using high doses of ionizing radiation to effectively target and destroy cancer cells [1, 2]. However, the high-energy photons used in radiotherapy, typically ranging from 1.25 to 25 MeV (mega-electron Volt), necessitate robust shielding to protect medical personnel and the surrounding environment from unintended exposure. As a result, photon shielding plays a critical role in ensuring the safe operation of radiotherapy and other types of facilities [3].

The interaction of photons with matter is governed by several mechanisms, including photoelectric absorption, Compton scattering, and pair production [4]. These interactions depend on both the energy of the incident photons and the properties of the shielding material. Consequently, the development and selection of materials for photon shielding require a detailed understanding of their physical, chemical, and radiation-attenuating properties [5-7]. Among these properties, density, atomic number (Z), and structural composition are particularly influential in determining a material's effectiveness against high-energy photons. Ordinary concrete is frequently employed as a material for radiation shielding, particularly against photons (X-rays and gamma rays), due to the following characteristics [8-10]:

i. The density of ordinary concrete (approximately 2.30–2.50 g/cm³) makes it efficient at attenuating photon radiation. Higher material density increases interactions with photons, thereby reducing their intensity.
ii. Ordinary concrete consists of aggregates bound by cement, and the diversity of its constituent materials provides a wider range of atomic numbers.
iii. Its composition, which includes elements like hydrogen, oxygen, silicon, and calcium, facilitates the absorption of photons through mechanisms such as the photoelectric

effect (at lower photon energies), Compton scattering (at intermediate energies), and pair production (at higher energies).

iv. Water molecules within concrete, either as bound water in the cement or free water in its pores, contribute to photon attenuation, with hydrogen being particularly effective in energy reduction via Compton scattering.

v. Concrete is readily available, cost-effective, and suitable for large-scale applications when compared to alternative shielding materials.

vi. It serves as both structural and shielding material, offering a dual-purpose solution for facilities such as nuclear power plants, radiotherapy centers, and research laboratories.

vii. Ordinary concrete's shielding capabilities can be enhanced by incorporating additional materials to improve its effectiveness against high-energy photons.

A wide range of materials has been investigated for use in constructing the walls of rooms housing high-energy photon sources [8, 9, 11-25]. Traditional shielding materials, such as lead and concrete, have long been employed due to their high density and cost-effectiveness. However, the demand for enhanced performance, reduced weight, and environmental sustainability has spurred research into new materials. Recent research has explored the incorporation of silicates, oxides, ceramics, and advanced concrete composites to optimize shielding properties [13-25]. Such innovations aim to optimize shielding while meeting the structural and economic requirements of modern radiotherapy facilities.

Among the materials investigated for photon shielding, titanium dioxide (TiO_2) and tungsten dioxide (WO_2) stand out not only for their high density (4.23 g/cm³ for TiO_2 and 10.80 g/cm³ for WO_2), but also for their unique physicochemical properties. TiO2 is known for its excellent chemical stability, non-toxicity, and high refractive index, making it suitable for long-term structural applications. WO_2, on the other hand, exhibits remarkable radiation resistance, thermal stability, and superior mechanical strength, enhancing the durability and shielding performance of composite materials. These properties, combined with their

availability and ease of incorporation into concrete matrices, make TiO_2 and WO_2 promising candidates for advanced photon shielding applications. The shielding effectiveness of these composites is assessed using the National Institute of Standards and Technology (NIST) XCOM database [26] to calculate key shielding quantities in the 1-10 MeV photon energy range. By assessing the feasibility of using these materials for constructing radiotherapy facility walls, this work aims to contribute to the development of safer and more efficient shielding solutions for high-energy photon applications, mainly in radiotherapy [3].

2. MATERIALS AND METHODS

This work utilized computational modeling to analyze the physical quantities of interest. Photon energy-dependent attenuation was modeled over the broad 1-10 MeV energy range to derive key quantities related to radiation shielding against high-energy photons. This range was chosen because it includes energy levels relevant for medical and industrial application of radiation shielding. Concrete mixes incorporating two types of metal oxides, namely titanium dioxide (TiO_2) and tungsten dioxide (WO_2), were analyzed to determine their impact on photon attenuation properties. A standardized conventional concrete mix (with a compressive strength of 25 MPa) was selected, consisting of a ratio of 1 part of Portland cement, 2 parts of sand, and 3 parts of gravel (by volume). This selection represents a commonly used mixture in construction, ensuring comparability with baseline data. TiO_2 and WO2 partially replaced gravel in proportions of 17%, 33%, and 50% by volume. Cement and sand were deliberately kept constant across all samples, while water content (after drying) was maintained at approximately 20% of the cement mass [10]. This design minimizes variables and enables a focused investigation of the oxides' effects. Thus, a total of six composite samples were considered and analyzed: three with TiO2 (samples Ti1, Ti2, and Ti3) and three with WO2 (samples W1, W2, and W3). The physical and compositional characteristics of these samples

were documented meticulously. The composition of each sample, along with its mass fractions and density, is summarized in Table 1.

Mass attenuation coefficients for each sample were computed using the reliable NIST XCOM database [26]. This database is widely recognized as a standard reference for photon interaction cross-sections, ensuring high accuracy in the results. The NIST XCOM database provides photon interaction cross-sections, including scattering, photoelectric absorption, and pair production, for individual elements as well as for custom compounds and mixtures.

Table 1: Composition and density of concrete samples analyzed.

Sample	Cement [%]	Sand [%]	Gravel [%]	Water [%]	Oxide [%]	Density [g/cm^3]
Ti1 (TiO_2)	16.71	28.03	29.11	3.34	22.80	2.80
Ti2 (TiO_2)	15.44	25.90	13.45	3.09	42.13	3.03
Ti3 (TiO_2)	14.35	24.06	0	2.87	58.72	3.26
W1 (WO_2)	12.34	20.70	21.50	2.47	42.99	3.79
W2 (WO_2)	9.33	15.65	8.13	1.87	65.02	5.02
W3 (WO_2)	7.50	12.58	0	1.50	78.41	6.24

The following set of equations was carefully applied to derive key shielding parameters. The mass attenuation coefficient is given by

$$\mu_m = \frac{\mu}{\rho}, \tag{1}$$

where μ is the linear attenuation coefficient and ρ is the density of the medium traversed by the photons. Considering the Lambert-Beer law [27] and the definition of tenth-value layer (TVL, thickness of the material that reduces the photon intensity by 10), TVL can be expressed as

$$TVL = \frac{\ln 10}{\rho . \mu_m}. \tag{2}$$

Another critical parameter is the mean-free path (MFP), which represents the average distance a photon travels without interacting with the material,

$$MFP = \frac{1}{\rho . \mu_m}. \quad (3)$$

Finally, the radiation protection efficiency (RPE), is defined as the efficiency of shielding materials in reducing radiation exposure. RPE is computed using the equation

$$RPE = (1 - e^{-\mu x}) \times 100\%, \quad (4)$$

where x is the thickness of the material traversed by the photons.

To handle and analyze the physical quantities of interest, a custom-built computational program written in Fortran was employed. This program provides robust numerical capabilities, ensuring precise data manipulation, accurate computation, and consistent results across all the derived shielding parameters. The calibration of the Fortran program was initially validated through manual calculations of the parameters for select cases, which were then compared with the results generated by the program. The consistency between the manual calculations and the simulated results was verified to ensure the accuracy of the model. Additionally, sensitivity tests were conducted to analyze the influence of variations in input parameters on the results. These tests helped identify the parameters that have the greatest impact on the outcomes and ensured the program's reliability across different scenarios.

3. RESULTS AND DISCUSSIONS

3.1. Mass attenuation coefficient

Figure 1 illustrates the variation in mass attenuation coefficients with incident photon energy for all samples. Up to 2 MeV, all samples exhibit similar values of mass attenuation coefficients, decreasing from 0.06501 to 0.04490 cm^2/g for Ti samples, and 0.06628 to 0.04509 cm^2/g for W samples. In this energy region, Compton scattering predominates, which is quite independent of the atomic number Z [4]. At higher photon energies, pair production significantly contributes to the total photon cross-section. Since pair production

depends on Z^2, the samples made with some parts of WO_2 exhibit higher mass attenuation coefficients (W3 > W2 > W1). Pair production is proportional to photon energy and Z^2, and thus the mass attenuation coefficients present a slight increase from 6 to 10 MeV for the densest samples containing WO_2.

At 4 MeV photon energy the mass attenuation coefficient of the W3 sample (78.4% of WO_2 in mass, see Table 1) is 2.4% higher than the value for the W2 sample (65% of WO_2 in mass), and is 6.5% higher than the value for the W1 sample (43% of WO_2 in mass). At 10 MeV photon energy, an increase in the differences among the mass attenuation coefficients can be observed; the mass attenuation coefficient for the W3 sample is 7.9% greater than that for W2 and is 22% greater than the value for W1. We can also notice that at 4 MeV the mass attenuation coefficient for the W3 sample is 16.8% greater than the value for the Ti3

Figure 1: The mass attenuation coefficient as a function of the photon energy for the 6 concrete samples incorporated with titanium dioxide (Ti1, Ti2, Ti3) and tungsten dioxide (W1, W2, W3).

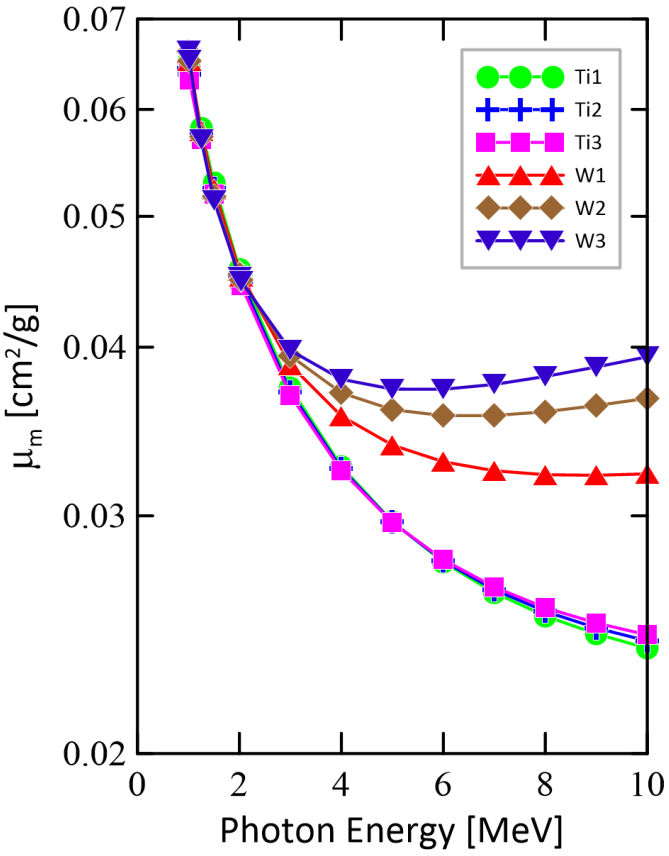

Source: The authors.

sample (58.7% of TiO_2 in mass). At 10 MeV the mass attenuation coefficient for the W3 sample is 60.7% higher than the value for the Ti3 sample. These findings suggest that the incorporation of tungsten dioxide in concrete may be a better choice to be used for shielding for a variety of applications such as medical, nuclear and research facilities as compared to concrete alone.

3.2. Mean-free path

In Figure 2 the mean-free path (MFP) is displayed as a function of the incident photon energy for all samples. A shorter MFP indicates greater interaction of photon with matter and reduced photon penetration in the medium. Figure 2 exhibits the general trend of growth of the mean-free path with photon energies for all samples. However, for the W samples and at high energies, there is a slight decrease in MFP due to the strong interaction via pair production. From the radiation protection point of view, the materials represented by the lower curves are more effective to shield photon beams. WO_2 samples consistently outperform TiO_2 samples, with W3 achieving the lowest MFP, particularly at high photon energies. For instance, at 4 MeV photon energy the MFP for the Ti1 sample is 8% superior to the MFP for the Ti2 sample; 15.7% superior to the value for the Ti3 sample; 47.5% above the value for the W1 sample; 103% above the value for the W2 sample, and 158% above the value for the W3 sample. At 10 MeV photon energy these percentages change, respectively, to 9.6; 19.2, 82.3; 174, and 266%.

3.3. Tenth-value layer

Figure 3 depicts the TVL as a function of the incident photon energy for the six samples as calculated by Equation (2). Also, again it can be seen the efficiency of the various samples in shielding photon beams. In the energy range analyzed, an overall increase of the TVL can be observed with photon energy for all samples. However, as already mentioned, a slight decrease in TVL for densest samples can be observed in the high-energy range accounting for the increase in pair production. Results indicate that samples formed by

concrete mixed with WO_2 are more effective in reducing the photon beam intensity. For instance, at 4 MeV the TVL for the Ti1 sample is 15.7 % higher than the TVL for the Ti3 sample and is 158% higher than the TVL for the W3 sample; at 10 MeV these differences in TVL increase, respectively, to 29.4 and 266%.

Figure 2: The mean-free path as a function of the photon energy for the six samples analyzed.

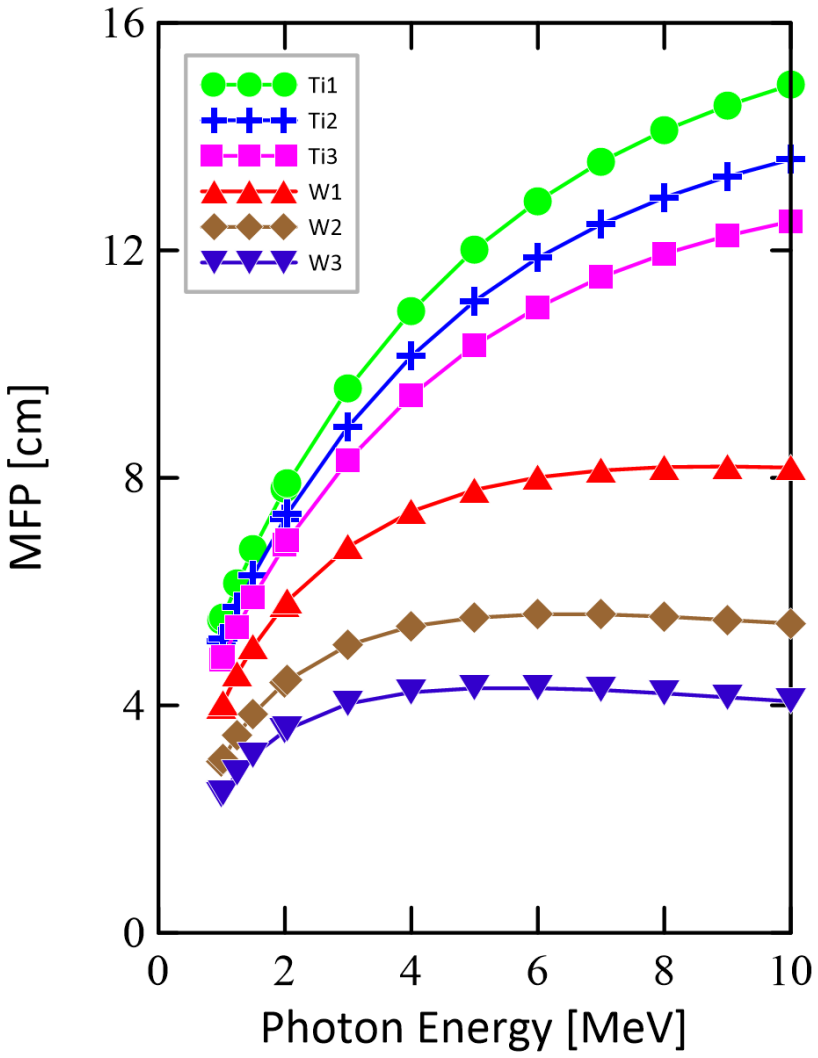

Source: The authors.

Figure 3: The TVL as a function of the photon energy for the six samples.

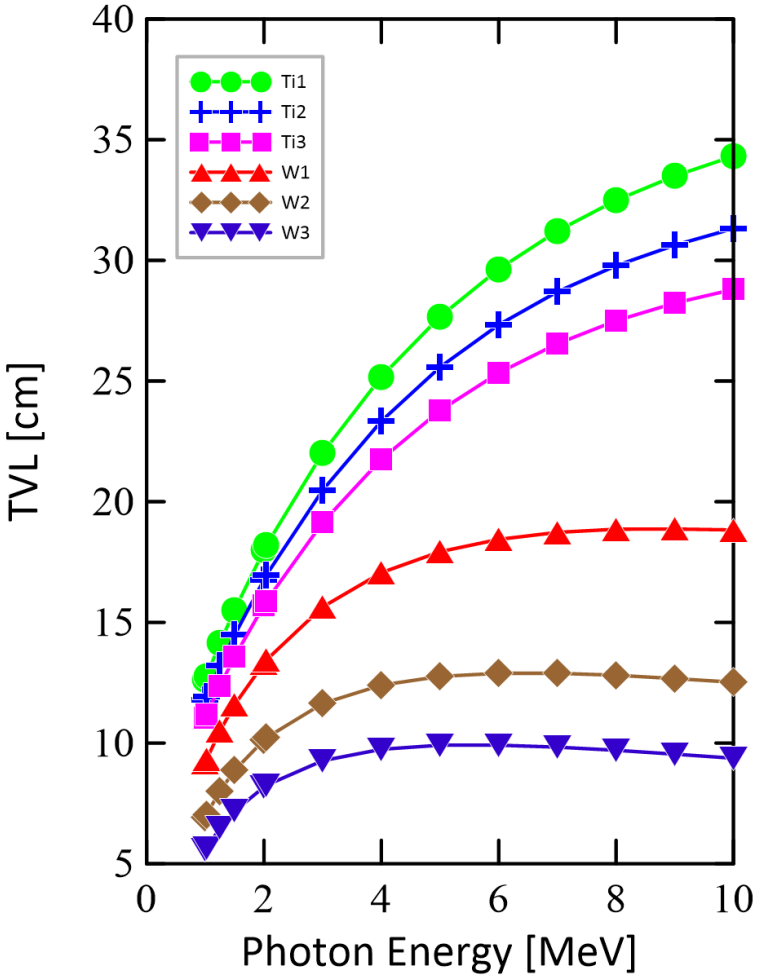

Source: The authors.

Figures 4 to 6 provide comparative analyses of TVL for the several samples analyzed, and also include ordinary concrete [3] and commercial glass [26], at fixed photon energies of 1.25, 6, and 10 MeV. Results consistently show that increasing concentrations of both oxides, TiO_2 and WO_2, in concrete improve shielding efficiency. For instance, at 1.25 MeV photon energy, the TVL for concrete exceeds the TVL for the Ti1 sample by 48% and surpasses the TVL for the W3 sample by 225%; similarly, at 1.25 MeV, the TVL for glass is 16% greater than the value for the Ti1 sample and 153% above the value for the W3 sample. These results suggest that these oxides incorporated into common concrete may be useful in photon beam shielding in radiotherapy facility rooms and nuclear systems. Data in Figures 5 (incident photon energy of 6 MeV) and 6 (incident photon energy of 10 MeV) present the same

behavior. At 6 MeV, differences of 46% and 273% can be observed, respectively, between TVL for concrete and TVL for Ti3 and W3 samples; at 10 MeV, these differences change, respectively, to 42 and 338%. These results highlight the superior shielding properties of these composites.

Figure 7 depicts the TVL as a function of the density of each sample of concrete mixed with WO_2 [W1 (3.79 g/cm^3), W2 (5.02 g/cm^3), and W3 (6.24 g/cm^3)] at the 1.25, 2, 4, 6, and 10 MeV photon energies. To allow a comparison data for common concrete (2.35 g/cm^3) are also shown [3]. For each photon energy the TVL decreases with increasing density, as a consequence of the increasing contribution of pair production to the total photon cross-section. For each sample, TVL increases with photon energy, also as a result of the increasing contribution of pair production at higher energy.

At 1.25 MeV photon energy, the TVL for concrete is double the TVL for the W1 sample and 2.25 times the TVL for the W3 sample. These differences change to 86% and 203%, 105% and 259%, 101% and 273%, 178% and 337%, respectively for the 2, 4, 6 and 10 MeV photon energy.

Figure 4: A comparison of the TVL values for the samples analyzed in this work, at a fixed photon energy of 1.25 MeV, is presented. The TVL values for common concrete and commercial glass are also included.

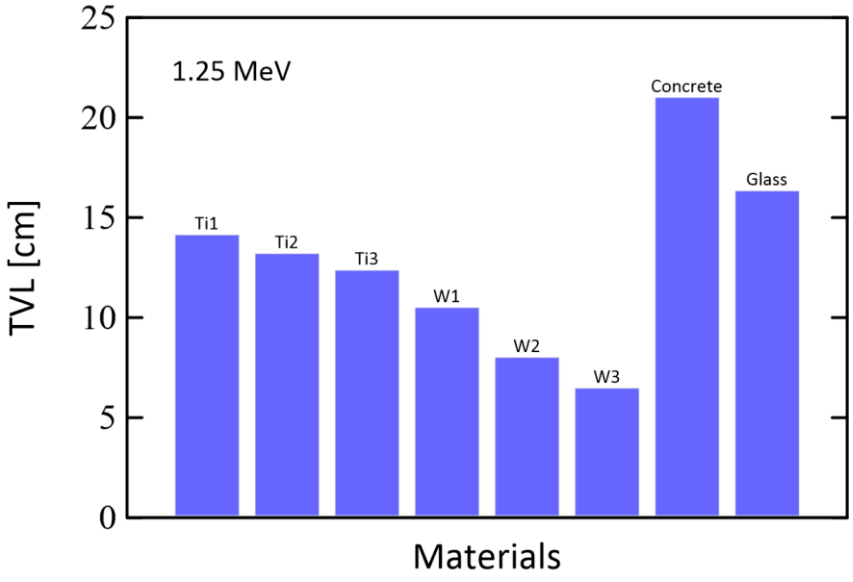

Source: The authors.

Figure 5: A comparison of the TVL values for the samples analyzed in this work, at a fixed photon energy of 6 MeV, is presented. The TVL values for common concrete and commercial glass are also included.

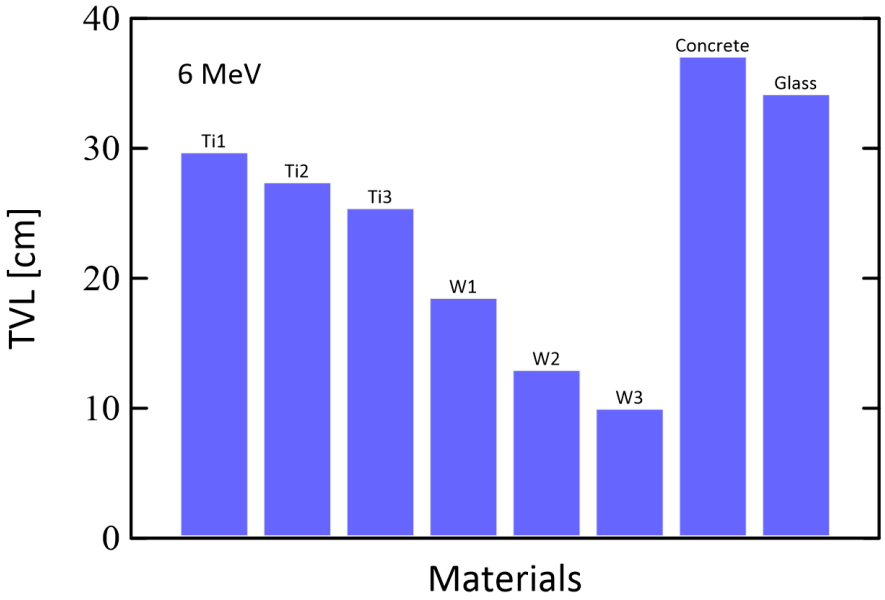

Source: The authors.

Figure 6: A comparison of the TVL values for the samples analyzed in this work, at a fixed photon energy of 10 MeV, is presented. The TVL values for common concrete and commercial glass are also included.

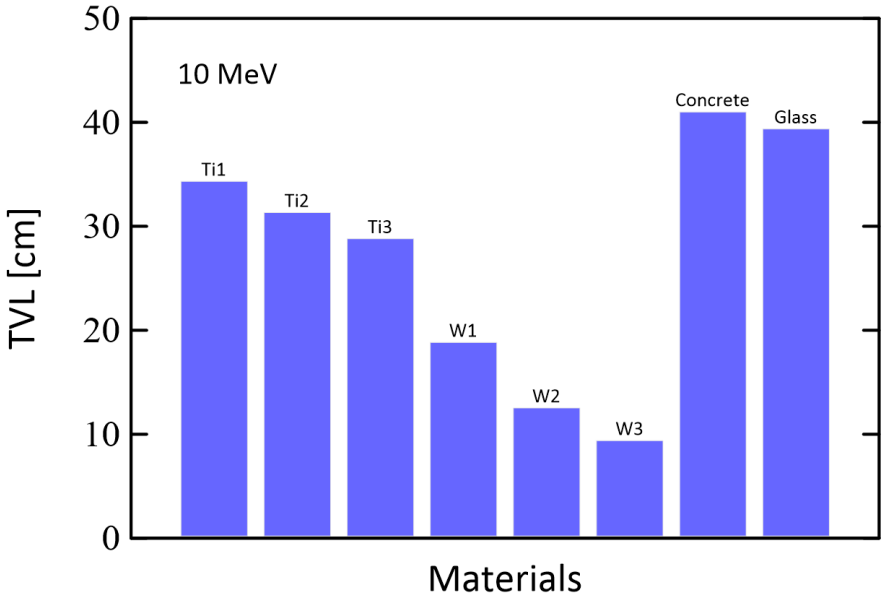

Source: The authors.

At 10 MeV photon energy and at higher density, TVL is lower than the TVL at 4 and 6 MeV. This reflects enhanced photon attenuation due to the combination of both high sample density and photon energy. Additionally, at 1.25 MeV photon energy, the TVL

for the lower-density W1 sample exceeds the TVL for the W2 sample by 31%, while the TVL for the W2 sample is 24% greater than that of the W3 sample. These differences change to 31% and 24%, 38% and 27%, 43% and 30%, 50% and 34%, respectively for photon energies of 2, 4, 6, and 10 MeV.

These results highlight the superior potential of using concrete samples mixed with WO2 for shielding rooms housing high-energy photon sources.

3.4. Radiation protection efficiency

Another important quantity that can be used to evaluate the effectiveness of a given material in reducing photon intensity is the radiation protection efficiency (RPE). Figure 8

Figure 7: The TVL as a function of density of each sample containing WO_2 (W1, W2, W3) incorporated into concrete for five different energies, from 1.25 to 10 MeV. TVL for ordinary concrete is also shown.

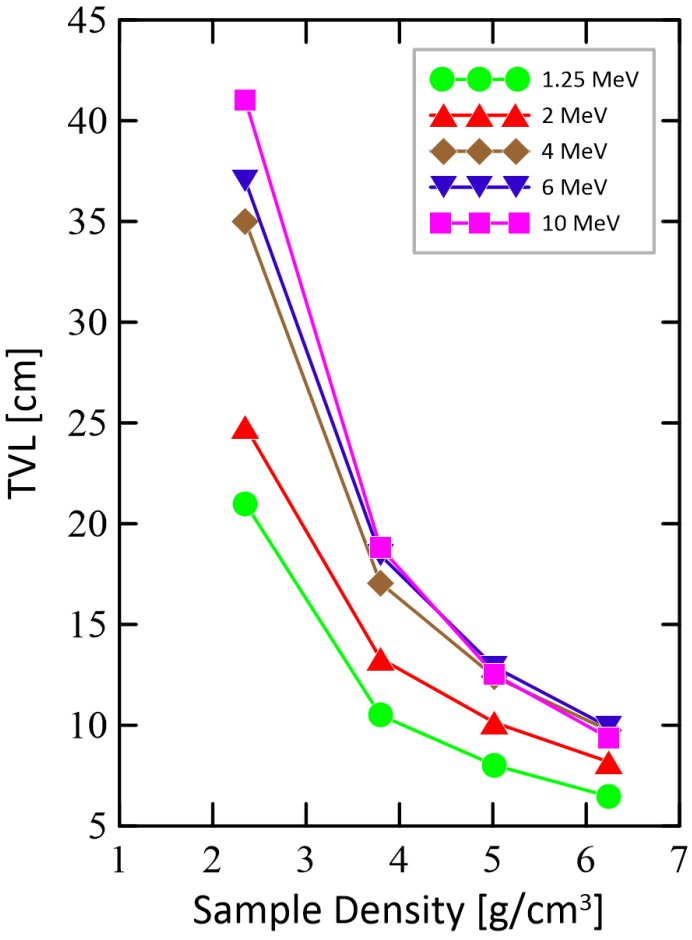

Source: Authors.

presents the result of RPE against photon energy for all six samples for a constant sample thickness of 10 cm. At lower energy levels (up to 2 MeV) efficiency is superior to 70% for all samples, and as energy increases there is a general decreasing of RPE for all samples. Decreasing of RPE is more pronounced for the Ti1 sample, which drops from 84% at 1 MeV to 49% at 10 MeV (- 72%); for the Ti3 sample these values change, respectively, to 88% and 55% (- 59%); and for the W3 sample these values change to 98% and 91% (- 7.6%). The highest RPE is observed for the W3 sample (78.4% of WO_2) with values greater than 91% for the entire energy range.

In Figure 9 the RPE is plotted against the sample thickness for all samples at a constant energy of 6 MeV. RPE presents a strong growth for all samples as thickness increases from 10 to 30 cm. From a thickness of 30 cm onwards the RPE is greater than or equal to 90% for all samples; for Ti1 sample RPE is 100% at 75 cm onwards; 70 cm onwards for Ti2 sample; 65 cm for Ti3; 45 cm for W1; 35 cm for W2, and 25 cm for W3 sample. These results reinforce the potential of analyzed samples (mainly W2 and W3) to be used in radiotherapy facility room shielding against photon radiation.

Figure 8: The radiation protection efficiency (RPE) as a function of the incident photon energy for all samples at a constant thickness of 10 cm.

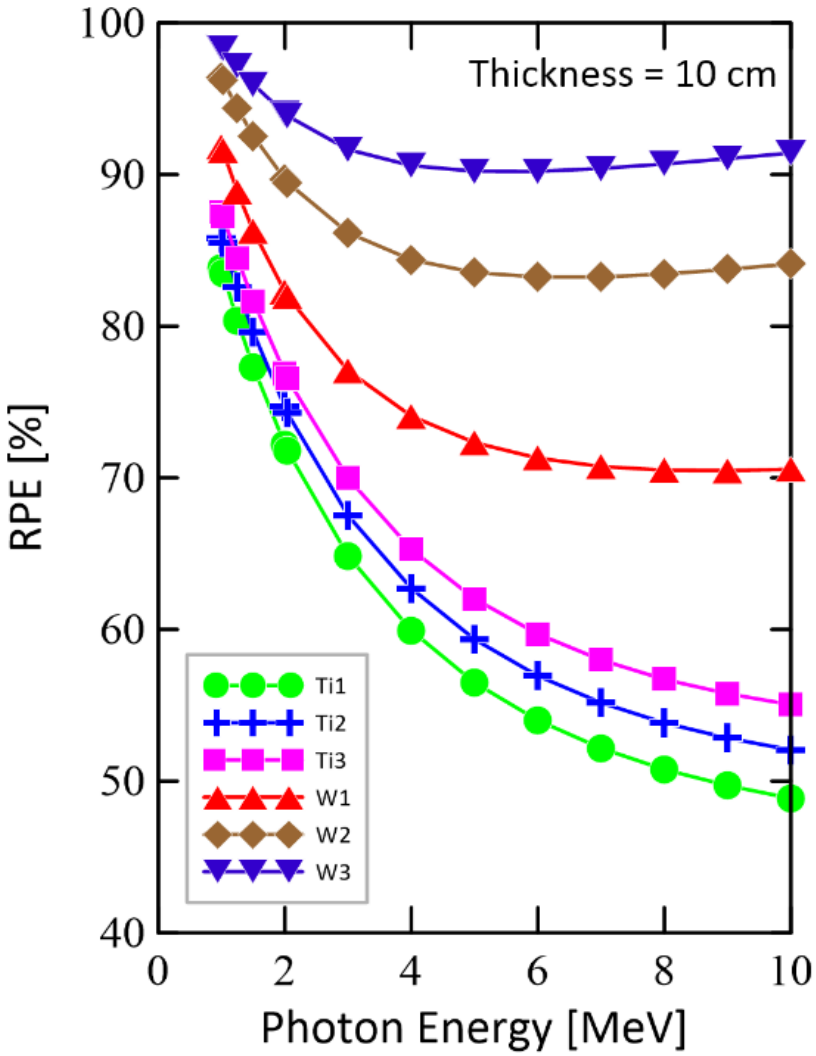

Source: The authors.

Figure 9: The radiation protection efficiency (RPE) as a function of the sample thickness at a constant energy of 6 MeV.

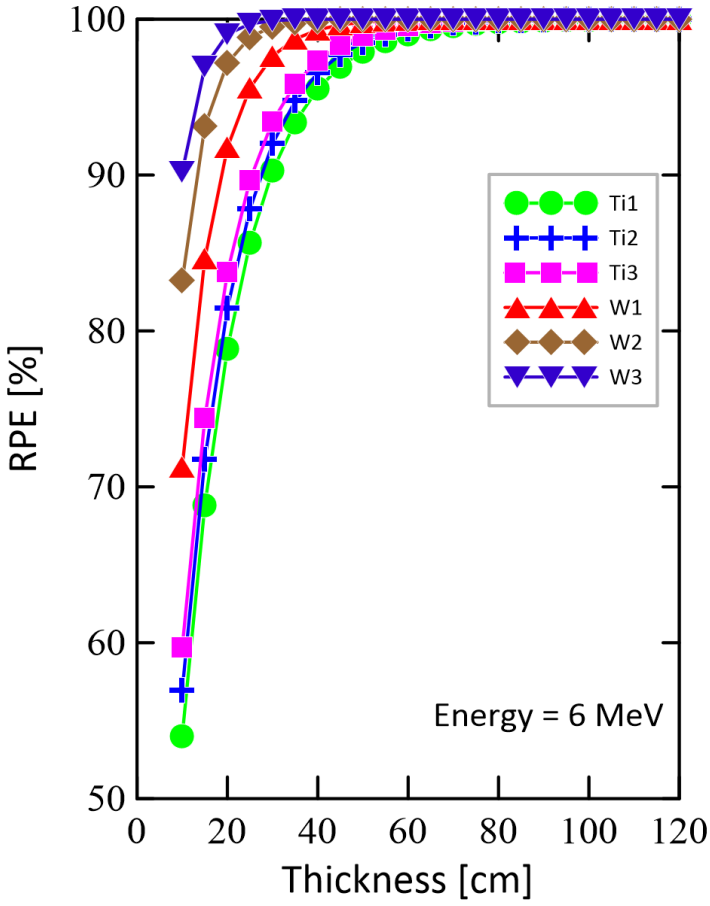

Source: The authors.

4. CONCLUSIONS

This study demonstrates the potential of titanium dioxide (TiO_2) and tungsten dioxide (WO_2) as effective additives for enhancing the photon shielding properties of concrete, particularly at high photon energies. While TiO_2 provides moderate improvement, WO_2 significantly enhances concrete shielding efficiency. These results suggest that both composites, mainly WO_2, could reduce wall thicknesses in radiotherapy facilities rooms while maintaining safety standards. Future work should focus on experimental validation and cost-benefit analyses to support the adoption of these materials.

ACKNOWLEDGEMENT

Cecília Borges Moreto would like to thank the CNEN for its partial financial support.

FUNDING

The authors declare no funding.

CONFLICT OF INTEREST

The authors declare that they have no conflicts of interest.

REFERENCES

[1] BASKAR, R.; YAP, S. P.; CHUA, K. L. M.; ITAHANA, K. The diverse and complex roles of radiation on cancer treatment: therapeutic target and genome maintenance. American Journal of Cancer Research, v. 2, n. 4, p. 372-382, 2012.

[2] BASKAR, R.; LEE, K. A.; YEO, R.; YEOH, K.-W. Cancer and radiation therapy: current advances and future directions. **International Journal of Medical Sciences**, v. 9, n. 3, p.193-199, 2012.

[3] National Council on Radiation Protection and Measurements. Structural Shielding Design and Evaluation for Medical Use of X-Rays and Gamma Rays of Energies Up to 10 MeV. NCRP Report No. 151, 2005.

[4] DE PAIVA, E. The Inverse-Square Law and the Exponential Attenuation Law Used to the Shielding Calculation in Radiotherapy on a High School Level. **The Physics Teacher**, v. 54, p. 239-242, 2016.

[5] KAÇAL, M. R.; AKMAN, F.; SAYYED, M. I.; AKMAN, F. Evaluation of gamma-ray and neutron attenuation properties of some polymers. **Nuclear Engineering and Technology**, v. 51, n. 3, p. 818-824, 2019.

[6] MOLLAH, A. S. Evaluation of Gamma Radiation Attenuation Characteristics of Different Type Shielding Materials used in Nuclear Medicine Services. **Bangladesh Journal of Nuclear Medicine**, v. 21, n. 2, p. 108-114, 2019.

[7] AL-BURIAHI, M. S.; ALZAHRANI, J. S.; OLARINOYE, I. O.; MUTUWONG, C; ELSAEEDY, H. I.; ALOMAIRY, S.; TONGUÇ, B. T. Effects of reducing PbO content on the elastic and radiation attenuation properties of germanate glasses: a new non-toxic candidate for shielding applications. **Journal of Materials Science: Materials in Electronics**, v. 32, p. 15080-15094, 2021.

[8] AKKURTA, I.; AKYILDIRIMA, H.; MAVIA, B.; KILINCARSLANB, S.; BASYIGITB, C. Gamma-ray shielding properties of concrete including barite at different energies. **Progress in Nuclear Energy**, v. 52, p. 620-623, 2010.

[9] WALY, EL-SAYED A.; BOURHAM, M. A. Comparative study of different concrete composition as gamma-ray shielding materials. **Annals of Nuclear Energy**, v. 85, p. 306-310, 2015.

[10] NEVILLE, A. M. Propriedades do concreto. Porto Alegre, RS: Bookman, 2016. p. 1–61. ISBN 978-85-8260-366-6.

[11] DONG, M.; XUE, X.; YANG, H.; LIU, D.; WANG, C.; LI, Z. A novel comprehensive utilization of vanadium slag: As gamma ray shielding material. **Journal of Hazardous Materials**, v. 318, p. 751–757, 2016.

[12] DE PAIVA, E. A study on the cost of concrete shielding in a standard radiotherapy facility room. **Brazilian Journal of Radiation Sciences**, v. 6, p. 1-18, 2018.

[13] DE PAIVA, E. An estimation of cost of concrete shielding in a radiotherapy room housing a clinical linear accelerator that produces high-energy photons. **Studies in Health Sciences**, Curitiba, v. 3, p. 1495-1507, 2022.

[14] GOUDA, M. M; ABBAS, M. I.; EID, M. H.; ZIEDAN, M. S.; IBRAHIM, M. A.; TAWFIK, M. M.; EL-KHATIB, A. M. Impact of micro/nano cadmium oxide on shielding properties of cement-ball clay matrix. **Scientific Reports**, v. 13, p. 18224, 2023.

[15] HAMAD, M.; DWAIKAT, N.; MHAREB, M.; SAYYED, M.; HAMAD, R.; ALAJERAMI, Y.; ALMESSIERE, M.; SALEH, G.; ALOMARI, A. H.; ZIQ, K. Influence of erbium on structural, and charged particles, photons, and neutrons shielding properties of Ba1–Er SnO3 perovskite ceramics. **Journal of Rare Earths**, v. 42, n. 4, 724–732, 2023.

[16] MHAREB, M. Optical, Structural, Radiation shielding, and Mechanical properties for borosilicate glass and glass ceramics doped with Gd2O3. **Ceramics International**, v. 49, n. 22, p. 36950–36961, 2023.

[17] HAMAD, M. K. Effects of bismuth substitution on the structural and ionizing radiation shielding properties of the novel BaSnBiO perovskites: An experimental study. **Materials Chemistry and Physics**, v. 308, p. 128254, 2023.

[18] SAYYED, M. Effect of WO_3 on the attenuation parameters of TeO2–La2O3-WO3 glasses for radiation shielding application. **Radiation Physics and Chemistry**, v. 215, p. 111319, 2023.

[19] SAYYED, M. I.; KAKY, K. M.; MHAREB, M. H. A.; AL-KEISY, A.; BAKI, S. O. Impact of CuO on TeO2–GeO2–ZnO–Al2O3–MgO glass system for ionizing shielding applications. **Journal of Materials Science: Materials in Electronics**, v. 34, n. 36, p. 2277, 2023.

[20] SAYYED, M. I.; MHAREB, M. H. A.; KAKY, K. M. Characterization of Mechanical and Radiation Shielding Features of Borosilicate Glasses Doped with MoO3. **Silicon**, v. 16, n. 5, 1955–1965, 2023.

[21] MORETO, C. B.; DE PAIVA, E. An initial study on common concrete, titanium dioxide and tungsten dioxide for shielding of a standard external photon beam radiotherapy room. **Studies in Health Sciences**, Curitiba, v. 5, n. 1, p.13-27, 2024.

[22] ALYAMI, J.; AL-HADEETHI, Y.; FALLATAH, O. A.; BIRADAR, S.; SAYYED, M.; ALMUTAIRI, F. Tailoring glass characteristics: Unveiling the impact of PbO and ZnO in Titanium-Barium borate glasses for advanced radiation protection. **Annals of Nuclear Energy**, v. 212, p. 111069, 2024.

[23] RUIZ, E. L. Radiation Shielding Analysis of Barium-Titanium-Borate Glasses Doped with Zinc Oxide. **Nexus of Future Materials**, v. 1, p. 80-85, 2024.

[24] HAMAD, M. K.; SAYYED, M. I.; MHAREB, M. H. A.; ELSAFI, M.; HANFI, M.Y.; MAHDI, M. A.; KHANDAKER, M. U. Effectiveness of barium oxide and zinc oxide in borate-based glasses for gamma radiation shielding. **Radiation Physics and Chemistry**, v. 229, n. 4, p. 112443, 2025.

[25] HAMED, M. K. Enhancing Ionizing Radiation Shielding Properties with PbO and ZnO Substitutions in B2O3-BaO-TiO2 Novel Glass System. **Radiation Physics and Chemistry**, v. 229, n. 4, p. 112499, 2025.

[26] NIST XCOM. XCOM: Photon Cross Sections Database. Available in: https://www.nist.gov/pml/xcom-photon-cross-sections-database. Accessed on: 10 dez. 2024.

[27] SWINEHART, D. F. The Beer-Lambert law. **Journal of Chemical Education**, v. 39, n. 7, p. 333-335, 1962.

LICENSE